Iraqi National Journal of Earth Science

www.earth.uomosul.edu.iq

Dynamics of Land Use and Land Cover Changes and Their Impact on Surface Temperature in Domkal Block, West Bengal, India

Woheeul Islam [1], **Md. Mustaquim** [2*], **Hasib Hasan** [3]

[1,2,3] *Department of Geography, Aliah University, Kolkata, India*

Article information

Received: 01- Feb -2025

Revised: 05- Mar -2025

Accepted: 16- Apr -2025

Available online: 01- Apr – 2026

Keywords:
Land Use,
Land Cover,
Land Surface Temperature,
Urban Heat Island,
Sustainability,

Correspondence:
Name: Md. Mustaquim

Email: mustaquim.md@gmail.com

ABSTRACT

Land is increasingly under pressure to meet the demands of a rapidly expanding population, so more resources are needed to maintain basic services and a high standard of living. This pressure leads to the reduction of natural vegetation and the formation of urban heat islands, a global concern linked to rising land surface temperatures, which, in turn, promotes unsustainable development. As a result, understanding the impact of land-use and land-cover changes (LULCC) on ecosystem sustainability has become critical in global change studies. This study utilizes Landsat satellite imagery processed with ArcGIS 10.5 and FRAGSTATS 4.2 to assess changes in land use and land cover, land fragmentation, and their relationship with land surface temperature (LST) and the normalized difference vegetation index (NDVI) in the Domkal block of Murshidabad District. The study assesses the magnitude and direction of these changes between 1991 and 2021 using change vector analysis. The findings reveal significant reductions in agricultural land (80.77 km²) and plantation areas (11.03 km²), offset by increases in built-up land (19.86 km²) and aquatic bodies (1.6 km²). Analysis of land surface temperature indicates an increase from 17-23°C in 1991 to 18-26°C in 2021. These changes are driven by demographic pressures, economic transformations, and reduced agricultural subsidies. The study emphasizes the need for sustainable land management practices, including the conservation of agricultural lands, efficient urban planning, and the implementation of conservation strategies to ensure ecological balance and promote socio-economic development.

DOI: 10.33899/injes.v26i2.60486,

ديناميكيات تغيرات استخدام الأراضي وتغطيتها وتأثيرها على درجة حرارة سطح الأرض في منطقة دومكال، غرب البنغال، الهند

وهيول إسلام [1]، محمد مستقيم [2*]، حسيب حسن [3]

[3،2،1] قسم الجغرافيا، جامعة عالية، كلكتا، الهند.

معلومات الارشفة

تاريخ الاستلام: 01- فبراير -2025

تاريخ المراجعة: 05- مارس -2025

تاريخ القبول: 16- ابريل-2025

تاريخ النشر الالكتروني: 01- ابريل-2026

الكلمات المفتاحية:

استخدامات الأرض،
الغطاء الأرضي،
درجة حرارة سطح الأرض،
الجزيرة الحرارية الحضرية،
الاستدامة،

المراسلة:

الاسم: محمد مستقيم

Email: mustaquim.md@gmail.com

الملخص

تتعرض الأراضي لضغوط متزايدة لتلبية احتياجات السكان المتزايدين بسرعة، مما يستدعي توفير المزيد من الموارد للحفاظ على الخدمات الأساسية ومستوى معيشي مرتفع. ويؤدي هذا الضغط إلى تقلص الغطاء النباتي الطبيعي وتكوّن الجزر الحرارية الحضرية، وهي مشكلة عالمية مرتبطة بارتفاع درجات حرارة سطح الأرض، الأمر الذي يُشجع بدوره على التنمية غير المستدامة. ونتيجة لذلك، أصبح فهم تأثير تغيرات استخدام الأراضي وتغطيتها على استدامة النظم البيئية أمرًا بالغ الأهمية في دراسات التغير المناخي العالمي. تستخدم هذه الدراسة صورًا فضائية من القمر الصناعي لاندسات، مُعالجة باستخدام برنامجي ArcGIS 10.5 و FRAGSTATS 4.2، لتقييم التغيرات في استخدام الأراضي وتغطيتها، وتجزئة الأراضي، وعلاقتها بدرجة حرارة سطح الأرض ومؤشر اختلاف الغطاء النباتي الطبيعي في منطقة دومكال التابعة لمقاطعة مرشد أباد. كما تُقيّم الدراسة حجم واتجاه هذه التغيرات بين عامي 1991 و2021 باستخدام تحليل متجه التغير. تكشف النتائج عن انخفاضات ملحوظة في الأراضي الزراعية (80.77 كم²) ومساحات المزارع (11.03 كم²)، يقابلها ارتفاع في مساحات الأراضي المبنية (19.86 كم²) والمسطحات المائية (1.6 كم²). ويشير تحليل درجة حرارة سطح الأرض إلى ارتفاعها من 17-23 درجة مئوية عام 1991 إلى 18-26 درجة مئوية عام 2021. وتعود هذه التغيرات إلى الضغوط الديموغرافية والتحولات الاقتصادية وانخفاض الدعم الزراعي. وتؤكد الدراسة على ضرورة اتباع ممارسات مستدامة لإدارة الأراضي، تشمل الحفاظ على الأراضي الزراعية، والتخطيط الحضري الفعال، وتطبيق استراتيجيات الحفاظ على البيئة لضمان التوازن البيئي وتعزيز التنمية الاجتماعية والاقتصادية.

DOI: 10.33899/injes.v26i2.60486, ©Authors, 2026, College of Science, University of Mosul.

Introduction

Satisfying the needs of a rapidly increasing population necessitates more resources to maintain essential services and a high quality of life, ultimately creating pressure on land. Changes in land use are required for economic development and social advancement; however, they are not without costs (Wu, 2008). New structures, stores, offices, and marketplaces are being constructed on land that was once used for agriculture, plantations, or forests. The majority of old homes in populated areas are demolished to make way for apartments. Backyard gardens are frequently cleared for structure expansion (Mustaquim and Islam, 2024). Recently, there is an increasing demand for information on actual land use/land cover (LULC) from planning, administration, and scientific institutions (Bety, 2013). The effects of land-use and land-cover changes (LULCC) on ecosystem sustainability are becoming significant in global change studies. Human activities are responsible for the most significant alterations to the Earth's surface. Changes in surface cover at local, regional, and global levels result in

modifications to energy, water, and geochemical fluxes, affecting natural resources and socio-economic activities (Islam et al., 2018). Changes in land use are mostly caused by human alteration of the Earth's surface, though biological processes also play a role (Islam et al., 2018; Kangabam et al., 2019; Naqvi et al., 2014). By reducing the amount of natural vegetation cover and creating urban heat islands, this encourages unsustainable development (Choudhury et al., 2019). Urban heat islands have emerged as a global issue in cities owing to elevated land surface temperatures. Factors influencing land-surface temperature (LST) encompass surface cover, urban morphology, and anthropogenic activities (Hoque and Lepcha, 2020). In order to study human-environment interactions, it is essential to comprehend the spatial-temporal variations of land surface temperature in urban settings. Accelerated urbanisation has caused a decline in vegetation within cities, with alterations in land use and cover contributing to elevated land surface temperatures in urban areas (Buyadi et al., 2013). Buyadi et al. (2013) and Ding and Shi (2013) observed that the urban microclimate is changed by rapid urban growth, which reduces vegetated areas and raises surface temperatures. LST intensity relates with land use and cover patterns including vegetation, water bodies, and built-up land (Ziaul and Pal, 2016). Comprehending this dynamic system is essential for LST and LULCC research, as well as for addressing social, economic and environmental issues. Accurately determining existing LULC contributions is essential for determining the impacts on LST changes. (Rehman et al., 2022). Thus, analysing the Earth's surface is crucial for understanding the interplay between human activities and natural events, thereby aiding in resource management and decision-making (Butt et al., 2015). The study employs FRAGSTAT software to assess land use fragmentation through landscape measurements. Diverse metrics derived from the geometric characteristics of landscape elements are frequently utilised in landscape analysis to provide quantitative assessments of intricate patterns (Dasgupta et al., 2009). The research investigates the impact of dynamic alterations in land use and cover on the environment through several indicators. The potential of satellite-based data to generate significant information for land use and land cover (LULC) is well acknowledged (Mishra et al., 2020). Researchers like Liu and Weng (2008), Das and Angadi (2020), Zhang et al. (2016), and Kafy et al. (2020) employed remotely sensed imagery, including Landsat images, to create land use maps, monitor changes and to generate surface temperature maps. Remote sensing, particularly via Landsat data, has demonstrated efficacy in distinguishing diverse terrain elements on a large scale (Butt et al., 2015). Landsat TM/ETM+/OLI data are frequently utilised for estimating land surface temperature (LST) and examining land-use change due to its spatial resolution (Choudhury et al., 2019). This study seeks to ascertain the magnitude and direction of land-use alterations over the preceding three decades. Furthermore, it analyses LST during this timeframe to establish the relation between land-use/land-cover alterations and LST conditions.

Materials and Methods

Study Area

The Domkal CD block is situated in Murshidabad District in the Indian state of West Bengal. It covers an area of 304.27 km². It is located at about 24.1412°N latitude and 88.5287°E longitude, with an elevation of 22 meters (72 feet) above mean sea level. According to the census of India, Domkal is a community development (CD) block located in the Domkal subdivision of the Murshidabad district (Fig. 1) in West Bengal, India. Domkal CD block is situated in the Bagri region of the district. The district is separated by the Bhagirathi River into two natural physiographic regions: Bagri on the east and Rarh on the west. The Jalangi and Bhairab Rivers also run through the area, characterized by low-lying terrain with many marshes and frequent flooding. According to the 2011 Indian census, the total population of the block was 363,976, all residing in rural areas, compared to 253,349 in 1991. Males made up 51% of the population, while females comprised 49%. Between 2001 and 2011, the population of the CD block increased by 16.78%. As per the 2011 census, the literacy rate in the CD block was 63.90%, with males at 64.47% and females at 63.31%. In 2011, cultivators constituted 15.74%

of the total workforce in the CD block, agricultural labourers made up 40.60%, home industry workers accounted for 14.28%, and other workers comprised 29.37%.

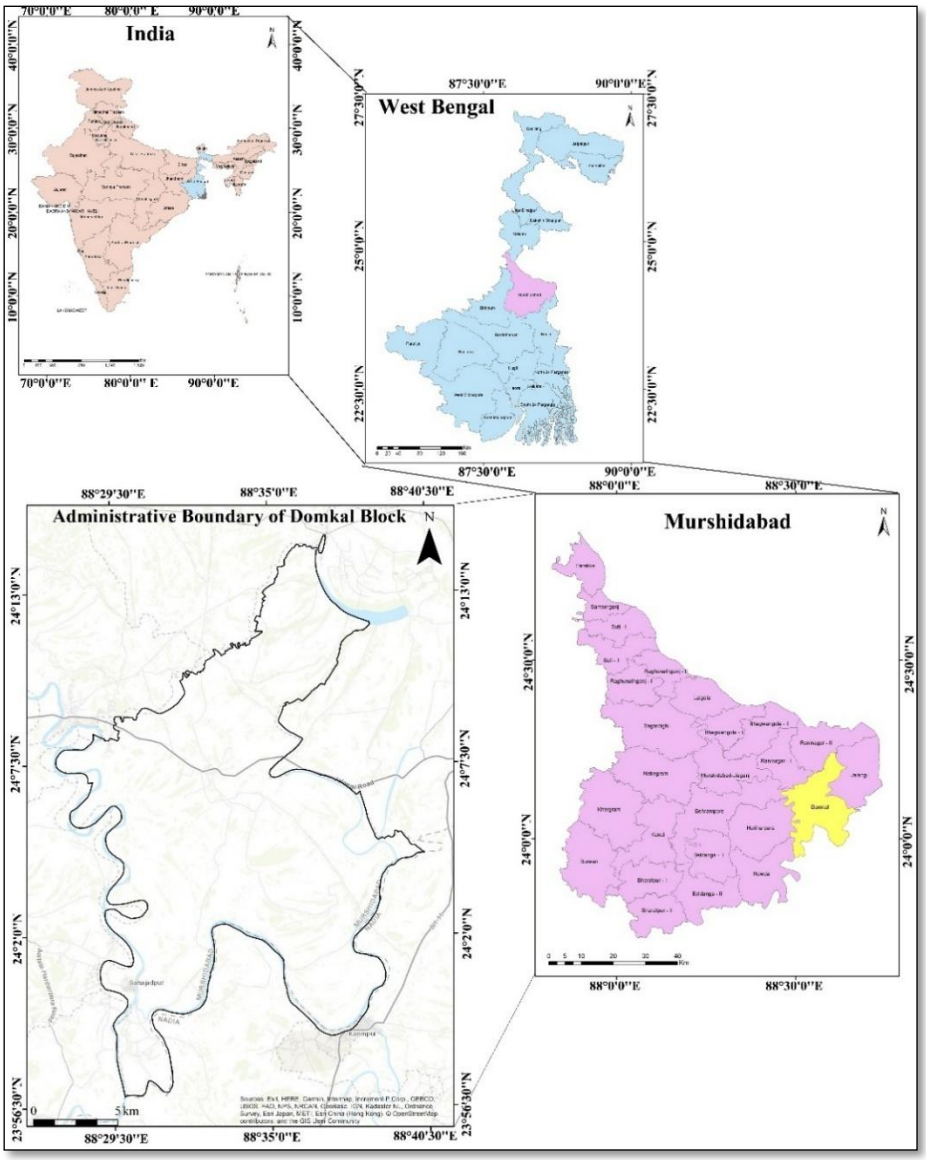

Fig. 1. Geographical location of the study area.

Data and Software

The availability of Landsat data sets has greatly facilitated regional-scale land use/cover classification and change detection (Hoque and Lepcha, 2020). Free satellite imagery is obtained from the USGS Earth Explorer website. For this study, multispectral images taken in the months surrounding each calendar year are used. Detailed information about the images can be found in Table (1) and Figure (2) illustrating the methodological framework of the study. To conduct the study, various software tools are utilized. ArcGIS 10.5 and ERDAS Imagine 2014 are employed for geospatial applications, FRAGSTAT is used for fragmentation analysis, and IBM SPSS 26 is applied for statistical analysis.

Table 1: Satellite Image Specifications Used in Analysis.

Year	Acquisition Date	Satellite	Sensor	Path/ Row	Resolution (m)	Projection
1991	02-02-1991	Landsat 5	TM	139/43	30	UTM-WGS84
2021	04-02-2021	Landsat 8	OLI/TIRS	139/43	30	UTM-WGS84

Source: USGS Earth Explorer

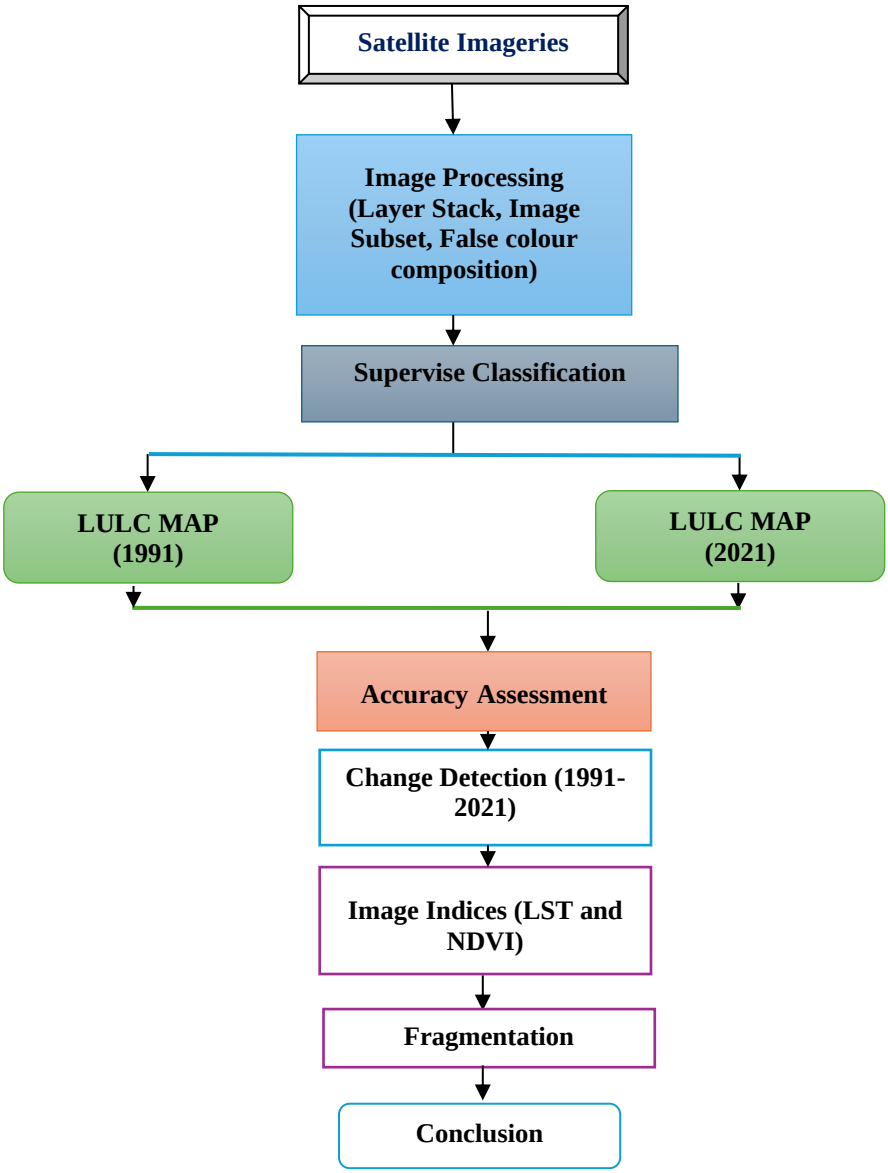

Fig. 2. Methodological Framework.

Image Classification

The primary goal of processing satellite images is to enhance the correlation between the data and the land cover it represents (Cheruto et al., 2016; Hua, 2017). Image classification seeks to derive thematic information from images of land use and land cover. ERDAS IMAGINE 2014 is utilized to derive thematic information from Landsat imagery. Land-use class signatures are obtained by visual image interpretation methods for each land-use category. Mosaicking and sub-setting are employed based on the area of interest (AOI). The application employs a pixel-based algorithm known as Maximum Likelihood Classification (MLC) for supervised classification, which is the predominant technique for analyzing land use and land cover changes. Using the normal distribution of the data for each class in each band, MLC determines the likelihood that a given pixel falls into a given category. Before classifying every pixel, a probability threshold needs to be established. After that, each pixel is allocated to the class that has the highest likelihood. Sisodia et al. (2014) and Bhatta (2011) offered extensive insights on maximum likelihood classification. Nelson and Khorram (2019) provided a comprehensive explanation of the supervised classification procedures in ERDAS IMAGINE in their book "Image Processing and Data Analysis with ERDAS IMAGINE". Recent studies by Gharaibeh et al. (2020), Alam et al. (2021), Saber et al. (2021), Mishra et al. (2020),

Chowdhury et al. (2020) and Roy and Kasemi (2021) employed supervised classification with the MLC technique to detect LULC changes. In this study, a set of training pixels is collected for each land use/cover category to create a class. After categorizing the satellite images, relevant adjustments (Recode) are made to generate the land use and land cover map. Water bodies, agricultural land, plantation and forest land, and built-up areas are the four land use and land cover categories that identified by the study (Table 2). ERDAS IMAGINE 2014 is used to assess accuracy, calculating the kappa coefficient and overall accuracy for each land use map. Local information and Google Earth maps are also used as references. The kappa coefficient, a reliable method for determining accuracy (Bose and Chowdhury, 2020), is 0.86 for 1991 and 0.89 for 2021, with overall accuracies of 92% and 98%, respectively. The entire procedure in detail is explained by Nelson and Khorram (2019) and Rwanga and Ndambuki (2017).

Table 2: Description of Identified Land Cover Classes.

LULC Classes	Descriptions
Agriculture (Crop Land)	Land is mostly utilized for the cultivation of food and fibre.
Built-up	An entirely artificial structure with a hard and non-porous surface.
Current Fallow (Crop Land without crop)	An area that hasn't grown crops for a while, so that it can grow again. The most common use for this product is in farming.
Plantation and Forest	The light vegetation is made up of areas where crops are grown, as well as a few small trees and some orchards.
Sand Bar	Sediment accumulations include sand that has been deposited in the riverine plane.
Water Bodies	There exist rivers, ponds, and inundated areas that are encompassed by surface water.

LST Extraction

Digital Number (DN) values are assigned to each pixel in an image to represent the intensity of electromagnetic radiation recorded by a digital sensor across different spectral bands at each location on the Earth's surface. The radiometric resolution of a sensor defines the range of DN values it can detect, meaning that DN values for the same substance may vary between sensors and over time due to environmental factors. Consequently, DN values must be converted into radiance and reflectance values. This transformation involves a series of steps (Fig. 3), which can be simplified using the "RS and GIS" plug-in introduced in QGIS Software. The "RS and GIS" plug-in, developed by Prathamesh Barane (2017) and available in the QGIS official repository, outlines these steps. In this work, guidelines for calculating Land Surface Temperature (LST) from images are followed, involving four stages to derive LST.

Step 1: Top of Atmospheric Radiance Calculation (TOA)

All entities above absolute zero (0 K) emit thermal electromagnetic radiation, enabling the thermal sensor to capture data that can be converted into sensor radiance. The spectral radiance was determined using the subsequent equation. (Choudhury et al., 2019; and Project Science Office, 2002):

Equation 1: For the Landsat 8 Image, there are two thermal bands (Band 10 and Band 11)

$$L\lambda = ML\lambda * Qcal + AL\lambda$$

Where: Lλ denotes the TOA spectral radiance; *Qcal* represents the individual pixel value; $AL\lambda$ signifies the radiance additive scaling factor for the respective band; $ML\lambda$ indicates the radiance multiplicative scaling factor for the corresponding band.

Equation 2: In the Landsat 5 TM image, Band 6 is the thermal band. The following formula has been used to convert the Landsat 5 TM image to radiance.

$$L\lambda = \left(\frac{Lmax\lambda - Lmin\lambda}{Qcal_{max} - Qcal_{min}} \times (Qcal - Qcal_{min})\right) + L_{min\lambda}$$

Where: *Qcal* represents the individual pixel value; $Qcal_{max}$ signifies the least quantized calibrated pixel value (often 1); $Qcal_{min}$ indicates the highest quantized calibrated pixel value (commonly 255); $L_{min\lambda}$ denotes the spectral radiance calibrated to $Qcal_{min}$ in W/(m²*ster*µm); $L_{max\lambda}$ indicates the spectral radiance normalized to $Qcal_{max}$ in W/(m²*ster*µm).

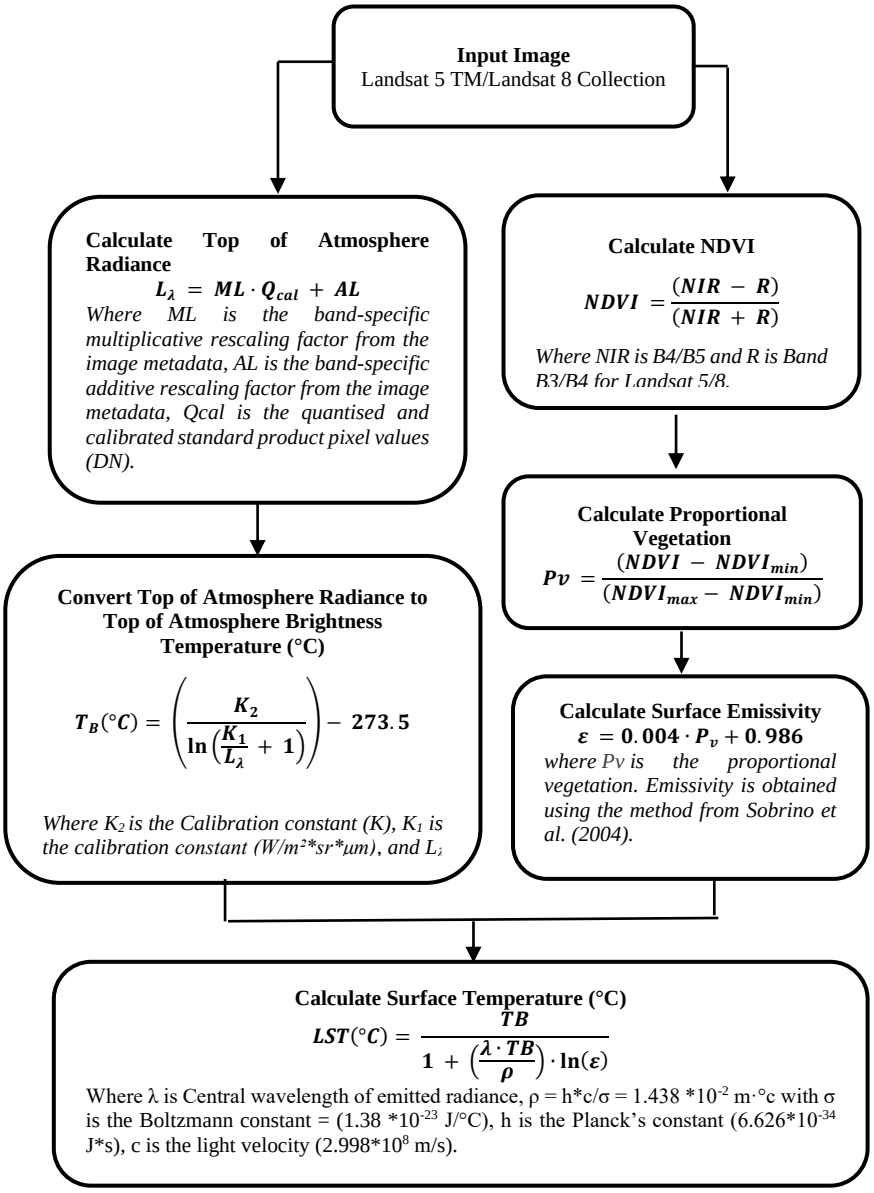

Fig. 3. Methodology for Computing Land Surface Temperature (LST) (Source: https://gis.stackexchange.com/)

Step 2: At-satellite brightness temperature calculation

The radiance measurements of the thermal band are subsequently transformed into at-satellite brightness temperature utilising the following equation (Artis and Carnahan, 1982; Hoque and Lepcha, 2020)

Equation 3:

$$T\lambda = \frac{K_2}{ln\left(\frac{K1}{L_\lambda + 1}\right)} - 273.15$$

Where: $T\lambda$ signifies the brightness temperature in degrees Celsius (°C), while $L\lambda$ indicates satellite radiation in W/(m²*ster*µm). *K1* and *K2* are calibration constants for pre-launch and are included in the metadata file.

Step 3: Emissivity calculation

Modifications for spectral emissivity (*e*) are required when correlating the temperature data acquired above to a black body. The modifications are predicated on land cover classification (Snyder et al., 1998) or by deriving emissivity values for each pixel from the vegetation proportion (*Pv*) data (Buyadi et al., 2013; Choudhury et al., 2019; Hoque and Lepcha, 2020).

Equation: 4

$$\boldsymbol{e = 0.004Pv + 0.986}$$

Where: *Pv* is the vegetation proportion computed using Equation 5.

Equation: 5

$$\left[\frac{\boldsymbol{NDVI - NDVI_{min}}}{\boldsymbol{NDVII_{max} - NDVI_{min}}}\right]^{\boldsymbol{2}}$$

Where: *NDVI*, or normalized difference vegetation index, is employed to evaluate the vegetation density within a designated area. The at-satellite reflectance of the near-infrared and red bands is employed to produce the *NDVI* image as per Equation 6.

The following formula of Townshend and Justice (1986) is used to calculate *NDVI*:

$$\boldsymbol{NDVI = \frac{(R_{NIR} - R_{RED})}{(R_{NIR} + R_{RED})}}$$

Step 4: LST calculation

To compute a reasonably realistic LST from at-satellite brightness temperature, the following equation is used (Choudhury et al., 2019; Hoque and Lepcha, 2020):

Equation: 7

$$\boldsymbol{LST = \frac{T\lambda}{1 + \left(\frac{\lambda \times T_{\lambda}}{\rho}\right) lne}}$$

Where: $T\lambda$ represents the at-satellite brightness temperature in degrees Celsius (°C); λ denotes the wavelength of emitted radiance in micrometers (μm); ρ is defined as h*c/j ($1.438*10^{-2}$ mK), where *j* is the Boltzmann constant ($1.38*10^{-23}$ J/K), *h* is Planck's constant ($6.626*10^{-34}$ Js), and *c* is the speed of light ($2.998*10^{8}$ m/s); *e* signifies land surface emissivity.

Image Indices

The normalized difference vegetation index (NDVI) is an instrument for evaluating the quantity of vegetation in a specified region. Equation (6) is employed to compute the NDVI. The "RS and GIS" plugin was utilized for this project. The NDVI scale ranges from -1 to +1, where low values signify the absence of vegetation and high values denote dense vegetation. Elevated values are potentially correlated with greater vegetation density.

Fragmentation analysis

Accurate and effective evaluation of landscape heterogeneity and connectivity at biologically significant scales is necessary for managing landscapes to promote socioeconomic development and preserve natural ecosystems that sustain biodiversity (Borthwick et al., 2020).

Table 3: Description of Matrices Used (Source: Adopted from McGarigal et al., 2002;and Mustaquim and Islam, 2023)

Abbreviation	Description	Justification
NP- Number of patches	Total number of patches in the Landscape	Fragmentation
PD- Patch density (per km')	Number of patches per unit area	Fragmentation
PLAND- Percentage of Landscape (%)	The proportion of the Landscape occupied by the patch type. When the number of the associated patch type (class) in the environment goes down, it gets closer to 0. PLAND is equal to 100 if the whole Landscape is made up of only one type of patch.	Fragmentation

LSI- Landscape shape index	Divided by the whole area and adjusted by a constant for a square standard, the landscape boundary and total edge within the Landscape	Aggregation
LPI- Largest patch index (%)	Each class's greatest patch's area corresponds to a percentage of the overall amount of land.	Dominance
MPS- Mean patch size (km^2)	Average patch size in each class, expressed in km.	Fragmentation
SHDI- Shannon's diversity index	SHDI equals minus the sum, a measure of diversity. When there is no diversity, it approaches 0, and it rises when more patch types are present.	Diversity

Both class-level and landscape-level indicators must be taken into account to fully understand how land-use change affects landscape fragmentation (Dewan et al., 2012). FRAGSTATS 4.2 is a spatial pattern analysis tool used to measure the heterogeneity and structure of landscapes Kamusoko and Aniya (2007); McGarigal et al. (2002); Sánchez Sánchez et al. (2021); and Singh et al. (2014). Determining landscape patterns, evaluating habitat fragmentation**,** and assessing biodiversity are the main uses of landscape metrics (Gardner et al., 1993; Herold et al., 2002; and Keitt et al., 1997). In this work, we have employed class-level and landscape-level measures from FRAGSTATS, a platform that provides information at the patch, class, and landscape scales (McGarigal et al., 2002). Patch-level measures denote distinct regions exhibiting identical characteristics, class-level metrics encompass all patches of a single type (LULC classes), and landscape-level metrics include all patches and classes within a designated area (Sertel et al., 2018). A single index is not enough to capture all of the complex patterns of land-use change because of its complexity. Therefore, multiple metrics (Table 3) are taken into account (Seto and Fragkias, 2005). We select metrics that consider the impact of changes in land use and cover on the fragmentation of the landscape as described by Dewan et al. (2012) and Kamusoko and Aniya (2007). Land-use change studies have extensively employed similar matrices in various research (Dewan et al., 2012; Kamusoko and Aniya, 2007; Sánchez Sánchez et al., 2021; Singh et al., 2014). The FRAGSTATS user manual McGarigal et al. (2002) and Mustaquim and Islam (2023) provides a comprehensive overview of the landscape measurements utilized.

Result and Discussions

Simple change analysis or degree of change does not adequately account for differences in land cover within and between periods. Consequently, change vector analysis is required to track the magnitude and direction of changes. In this study, ArcGIS 10.5 was utilized to generate the change transition matrix. Fig. 4 illustrates significant changes over time, while Table 4 indicates that agricultural land and plantation areas have decreased by 80.77 km^2 and 11.03 km^2, respectively. Conversely, built-up land and aquatic bodies have increased by approximately 19.86 km^2 and 1.6 km^2, respectively. The Domkal block covers roughly 311 km^2.

As shown in Table 5 and Fig. 5, nearly 44% of the land cover has changed in the last 30 years. Agricultural land is shrinking due to the expansion of plantations (14.37 km^2), built-up areas (13.03 km^2), and current fallow land cover (66.45 km^2). The area under current fallow has increased by around 70 km^2, predominantly from agricultural land (66.45 km^2). Due to the encroachment of agricultural land, the expansion of current fallow and built-up areas, the plantation area has decreased by 11.03 km^2. It is observed that the expansion of built-up areas, approximately 19.86 km^2, encroached significantly on agricultural land (13.03 km^2) and plantation cover (8.01 km^2). The increase in built-up areas and the decrease in agricultural and plantation areas are attributed to increasing population pressure. Factors such as the shift from traditional agricultural practices to other sectors, dependence on natural resources, reduction of subsidies, lack of credit systems, reliance on money lenders, reduction of government investment in agriculture, and the conversion of agricultural land to alternative uses have all contributed to the decline in agricultural land. These trends are clearly evident from Indian census statistics, and Figure (9) provides a visual representation of these demographic and economic changes. The nature and extent of changes among the defined land cover classes are clearly recognized in Figure (5).

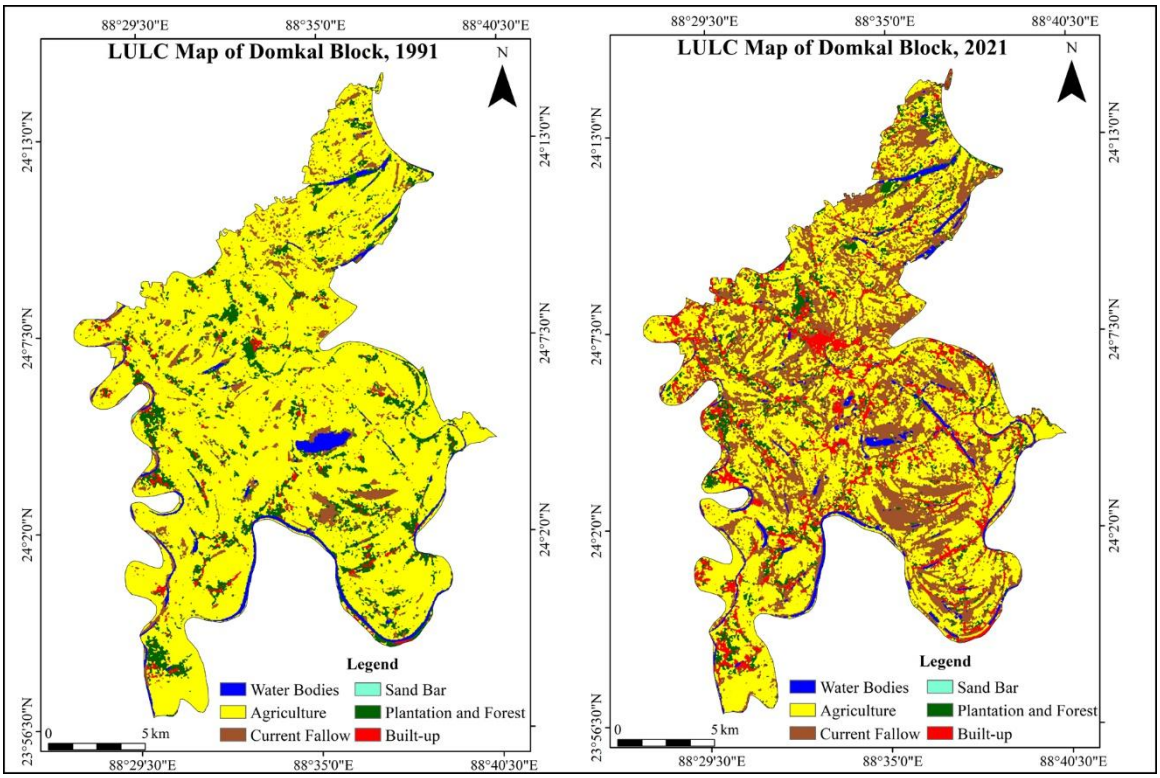

Fig. 4. Spatial Distribution of LULC Classes in Domkal Block

Table 4: Land Use and Cover Class Distribution in Domkal Block

Class Name	1991 (km^2)	2021 (km^2)	Relative Changes (km^2)
Water Bodies	8.42	10.02	1.60
Agriculture	245.33	164.56	-80.77
Current Fallow	18.76	89.08	70.32
Sand Bar	0.12	0.04	-0.08
Plantation and Forest	32.95	21.92	-11.03
Built-up	5.86	25.73	19.86

Table 5: Decadal Land Use and Cover Shifts: 1991-2021

Land Cover Class	**Water Bodies**	**Agriculture**	**Current Fallow**	**Sand Bar**	**Plantation and Forest**	**Built-up**	**Grand Total**
Water Bodies	4.91	1.30	1.61	0.01	0.33	0.23	**8.38**
Agriculture	2.02	149.12	66.45	0.03	14.37	13.03	**245.01**
Current Fallow	1.33	4.35	10.87	0.01	0.84	1.33	**18.72**
Sand Bar	0.00	0.04	0.04			0.04	**0.12**
Plantation and Forest	1.58	8.78	8.41	0	6.14	8.01	**32.91**
Built-up	0.14	0.79	1.63		0.23	3.07	**5.86**
Grand Total	**9.98**	**164.37**	**89.00**	**0.04**	**21.91**	**25.70**	**311.00**

Moreover, Figure 6 (a, b) reveals a substantial shift in the land surface temperature (LST) distribution over the 30-years period. The temperature range is 19.01-20°C, which was predominant in 1991 (Fig. 7), experienced a dramatic decline by 2021. Conversely, temperatures in the range of 21.01-22°C saw a significant increase, becoming the most extensive temperature category in 2021. This shift indicates a clear trend of rising land surface temperatures in Domkal block. The increase in higher temperature ranges (>20°C) and the corresponding reduction in lower temperature ranges (<20°C) suggest an overall warming trend in the area. This trend is concerning as it reflects potential impacts of climate change affecting local ecosystems, agriculture, and overall land use patterns. The pronounced increase (Fig. 7) in areas experiencing temperatures of 21.01-22°C and above underscores the need for climate adaptation and mitigation strategies to manage the rising temperatures and their effects on land use in Domkal block. Additionally, in 1991, temperatures varied from 17 to 23°C; however, in 2021, they grew to a range of 18 to 26°C, signifying a rise of 1°C in the minimum temperature and 3°C in the maximum temperature. The mean LST was obtained at 1,067 sample locations

to compare the mean significant difference of LST using a paired samples t-test with a significance level of 0.05. The histograms for both pre- and post-test scores and their differences show that the assumption of normality was not violated when comparing LST before (Mean, M = 19.61, Standard Deviation, SD = 0.017) and after (M = 21.14, SD = 0.021). The difference in LST from 1991 to 2021 is statistically significant (Table 6), with a *p*-value of less than 0.001 (two-tailed). Whereas, visual image analysis indicates that built-up areas, barren terrain, and agricultural land adjacent to rivers and barren land have high temperatures. The western side, due to riverine sand deposition, has a high temperature. The central and eastern regions also experience high temperatures due to the expansion of built-up territory and fallow land. Additionally, many new bricks kiln factories have been built in the last 30 years, contributing to high temperatures around agricultural land (Fig. 8). To create the scatter plot, 1,050 points are generated using the fishnet tool, and multi-values are added to each point to include LST and NDVI values (Fig. 6 c, d) for each unique location. This task is completed using ArcGIS 10.5 software. It is found that areas with low NDVI values have high temperatures. Therefore, in the scatter plot, the x-axis represents the NDVI value, while the y-axis represents the LST value, indicating that as the NDVI value decreases (Fig. 10), the temperature rises.

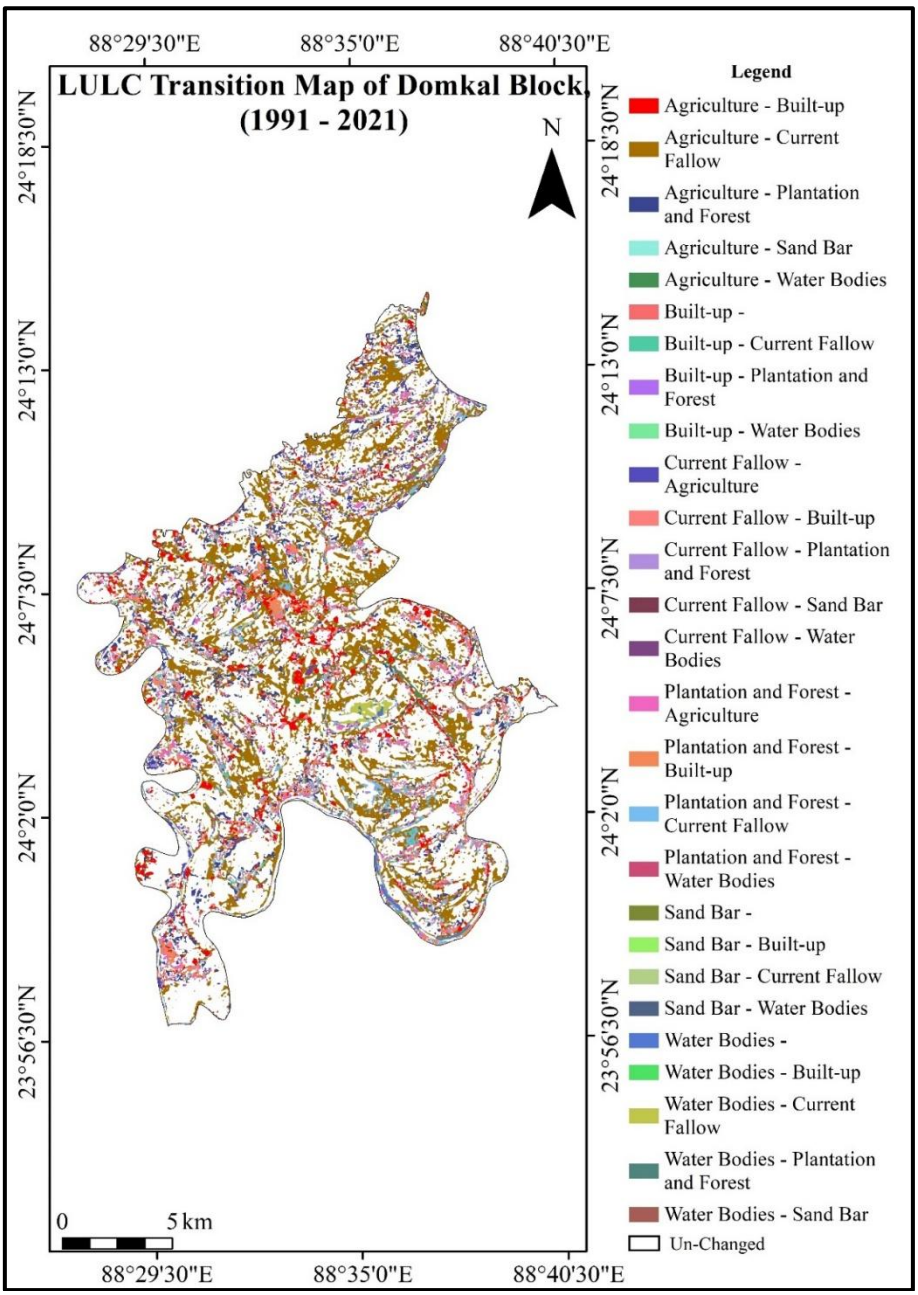

Fig. 5. Temporal transition map of land use/land cover in Domkal Block.

Table 6: Analysis of paired samples t-Test.

Paired Samples Test									
		Paired Differences					t	df	Sig. (2-tailed)
		Mean	Std. Deviation	Std. Error Mean	95% Confidence Interval of the Difference				
					Lower	Upper			
Pair 1	LST 1991 - LST 2021	-1.52	.78	.02	-1.57	-1.48	-63.53	1066.00	.00

Furthermore, Tables 7 and 8 display the Pearson correlation coefficients between LST and NDVI for the Domkal block in 1991 and 2021. A Pearson correlation coefficient of -0.466 signifies a moderate inverse association between LST and NDVI in 1991. Regions exhibiting higher land surface temperatures generally demonstrate decreasing vegetation density as indicated by NDVI. The substantial p-value (0.000) verifies that this correlation is statistically significant at the 0.01 level. In 2021, the Pearson correlation coefficient between LST and NDVI is -0.355. This continues to demonstrate an unfavourable association, though less pronounced than in 1991. The decline in the correlation coefficient indicates a weakening of the inverse link between temperature and vegetation density during the thirty-year span. The correlation is statistically significant as evidenced by the p-value of (0.000). Furthermore, our results emphasise the necessity for ongoing surveillance and administration of land surface temperatures and vegetation coverage. Comprehending the dynamic relationship between LST and NDVI helps guide sustainable land use practices and climate adaptation methods in the Domkal block.

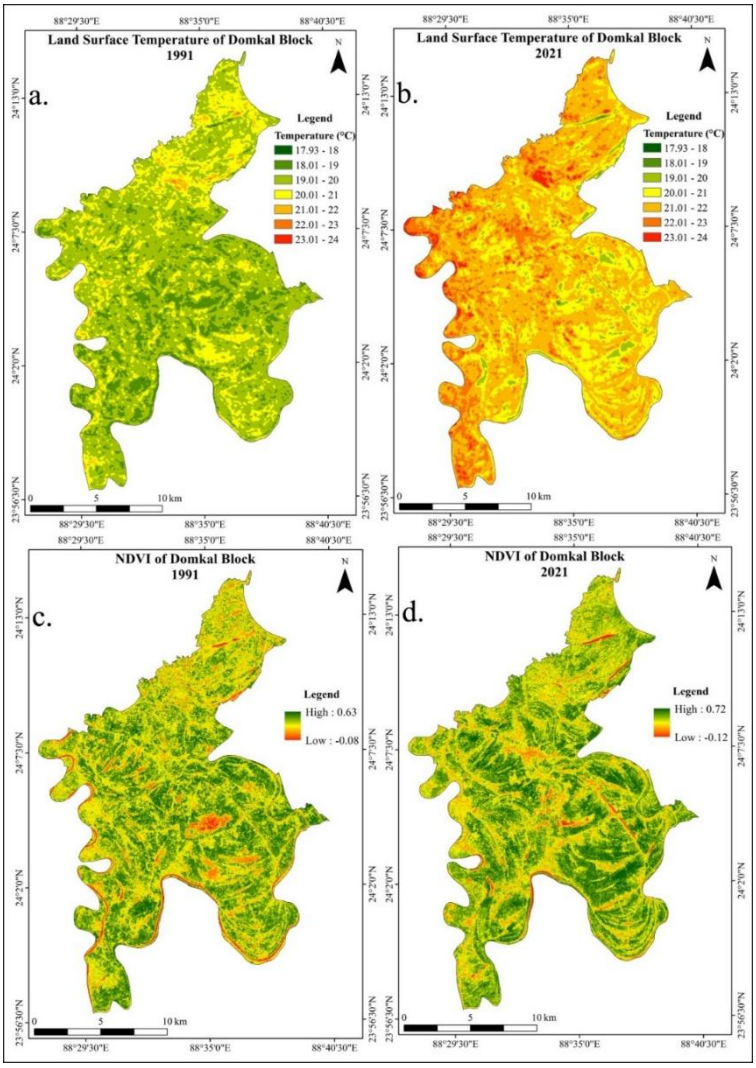

Fig. 6. LST and NDVI trends over decades: Domkal Block (1991-2021).

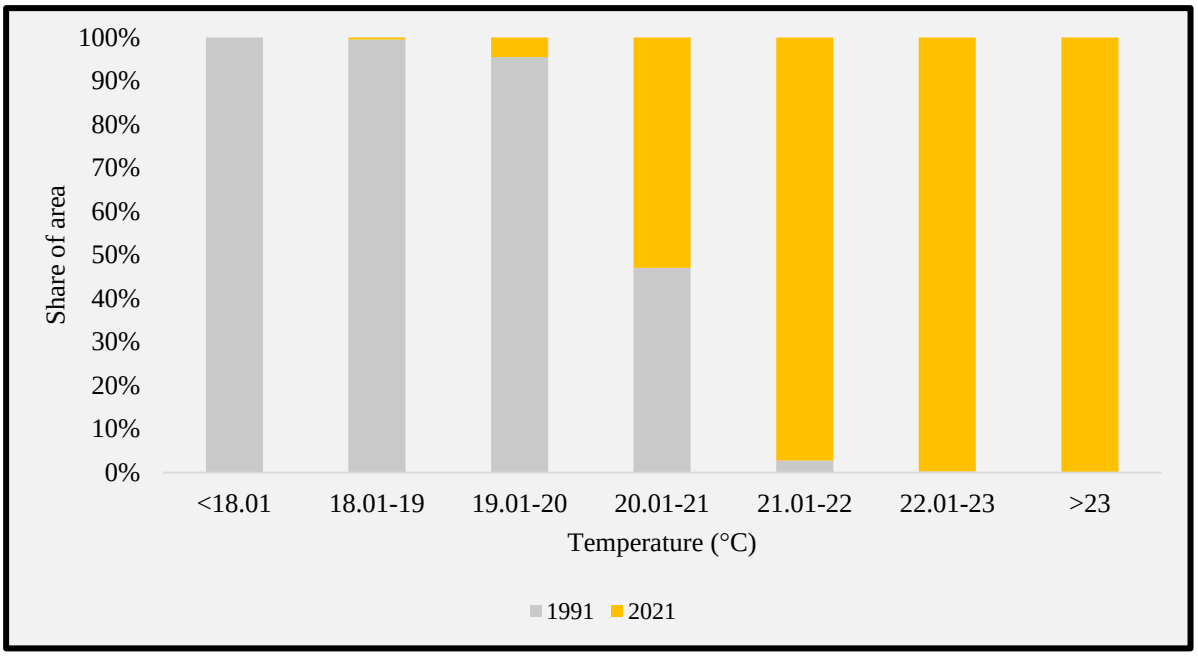

Fig. 7. Changes in LST distribution and area coverage in Domkal Block (1991-2021).

Table 7: Correlation Matrix of LST and NDVI of 1991.

	Correlations	LST (1991)	NDVI (1991)
LST (1991)	Pearson Correlation	1	-0.466**
	Sig. (2-tailed)		0.000
	N	1056	1056
NDVI (1991)	Pearson Correlation	-0.466**	1
	Sig. (2-tailed)	0.000	
	N	1056	1056
**Correlation is significant at the 0.01 level (2-tailed).			

Table 8: Correlation matrix of LST and NDVI of 2021.

	Correlations	LST (2021)	NDVI (2021)
LST (2021)	Pearson Correlation	1	-0.355**
	Sig. (2-tailed)		0.000
	N	1049	1049
NDVI (2021)	Pearson Correlation	-0.355**	1
	Sig. (2-tailed)	0.000	
	N	1049	1049
**Correlation is significant at the 0.01 level (2-tailed).			

Land Fragmentation Analysis by Matrices

In order to comprehend the fragmentation of land and the disturbances caused by human activities, two types of matrices are employed: class level matrix (Table 9) and landscape level matrix. The current study utilizes six class level and one landscape level matrix called SHID. The investigation of fragmentation in the study region between 1991 and 2021 demonstrates notable alterations in several land cover categories. For agriculture, the percentage of landscape (PLAND) decreases from 78.77% to 52.49%, accompanied by an increase in the number of patches (NP) from 289 to 1,261 and patch density (PD) from 0.93 to 4.05. This indicates substantial fragmentation, further evidenced by a decrease in mean patch size (MPS) from 84.89 km^2 to 12.96 km^2, a reduction in the largest patch index (LPI) from 75.57% to 6.89%, and an increase in the landscape shape index (LSI) from 26.89 to 55.72. These changes suggest that agricultural land has become more fragmented and less dominant, with patches becoming more irregular in shape. Built-up areas have expanded significantly, with PLAND increasing from 1.88% to 8.31%. The NP rose from 629 to 1,708, and PD increased from 2.02 to 5.48**,** indicating urban growth. The MPS also increased from 0.93 km^2 to 1.52 km^2, while the LPI grew from 0.07% to 0.47%. The LSI increased from 28.84 to 49.74**,** suggesting that built-up areas have not only grown in number but also in complexity and size**,** forming larger and more irregular

patches. Current fallow land has seen a substantial increase in PLAND from 6.02% to 28.75%**,** reflecting a shift in land use practices. The NP increased from 1,139 to 2,797, and PD from 3.66 to 8.98**,** indicating increased fragmentation. The MPS grew from 1.65 km^2 to 3.2 km^2, and the LPI rose from 0.4% to 2.65%. The LSI also increased from 38.1 to 66.65**,** showing that these fallow areas are becoming more prevalent, larger, and more complex in shape.

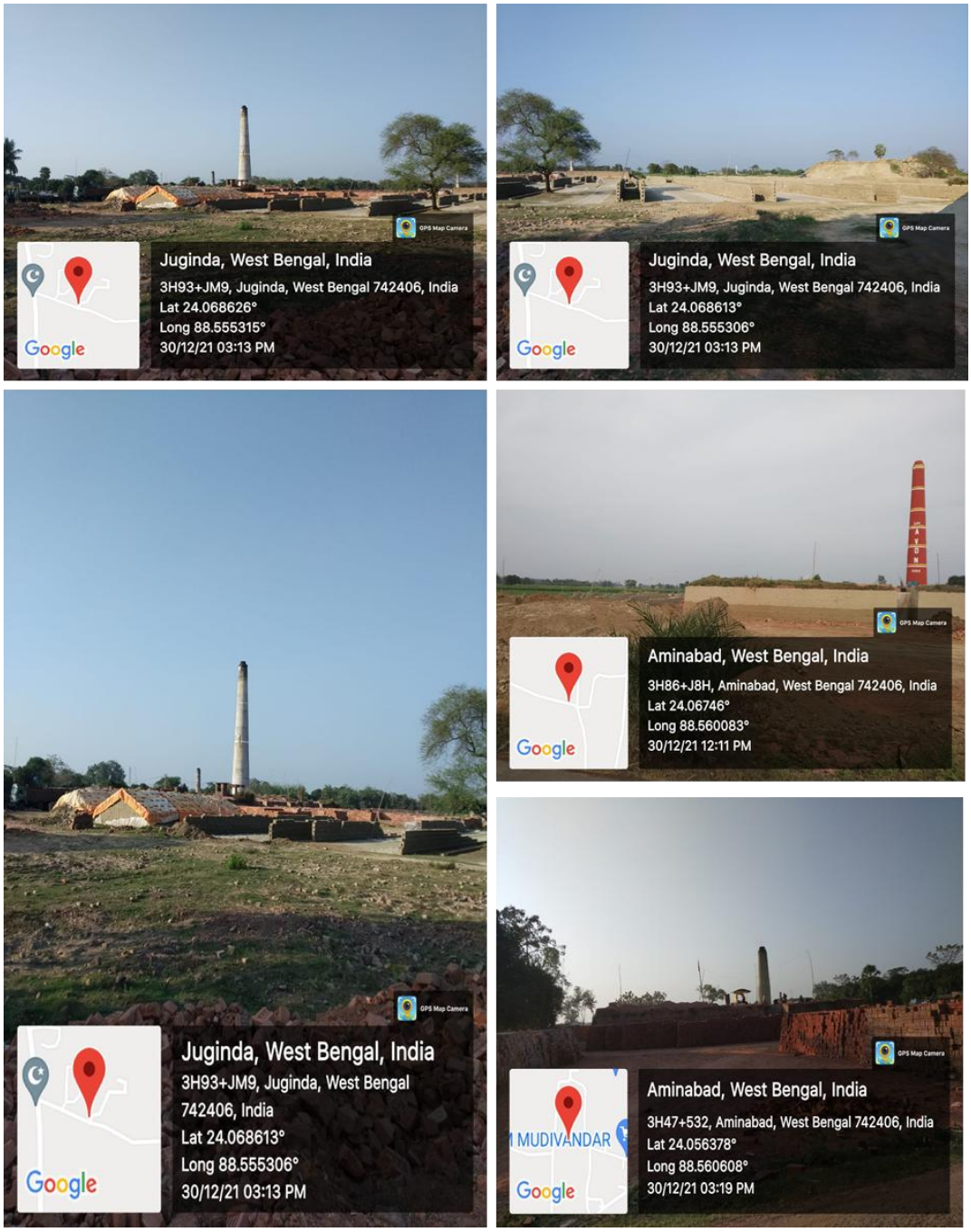

Fig. 8. Photographs showing brick kilns enclosed by agricultural land.

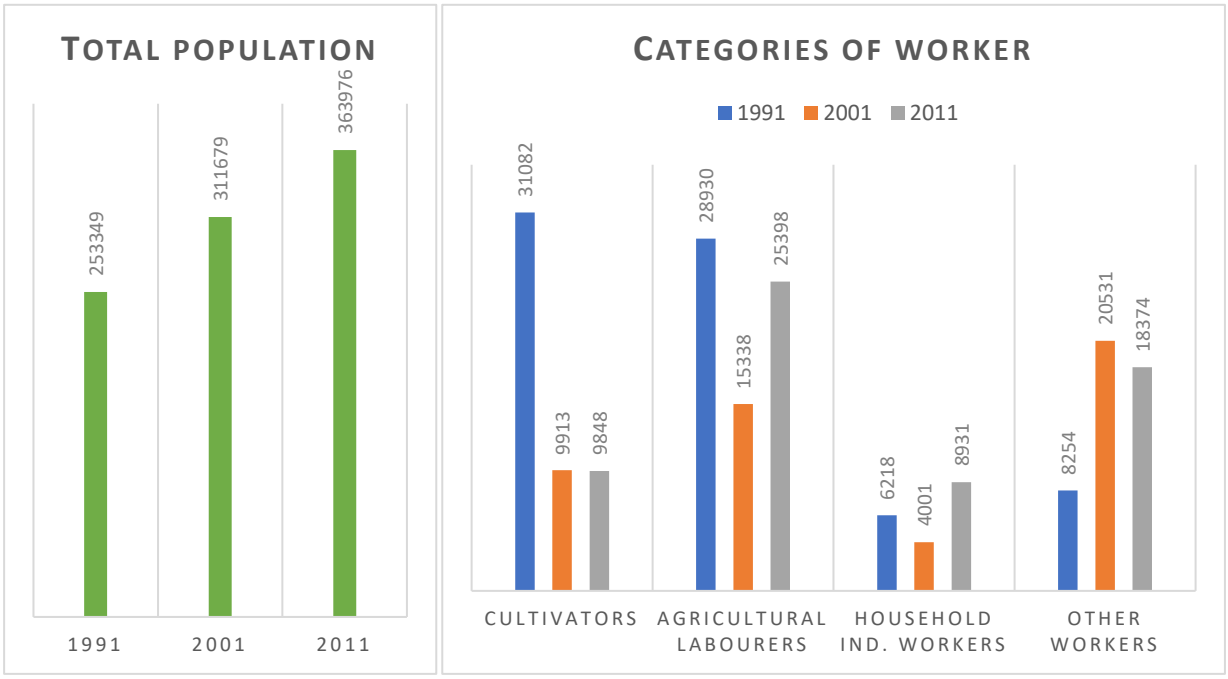

Fig. 9. Population and occupational structure in Domkal Block.

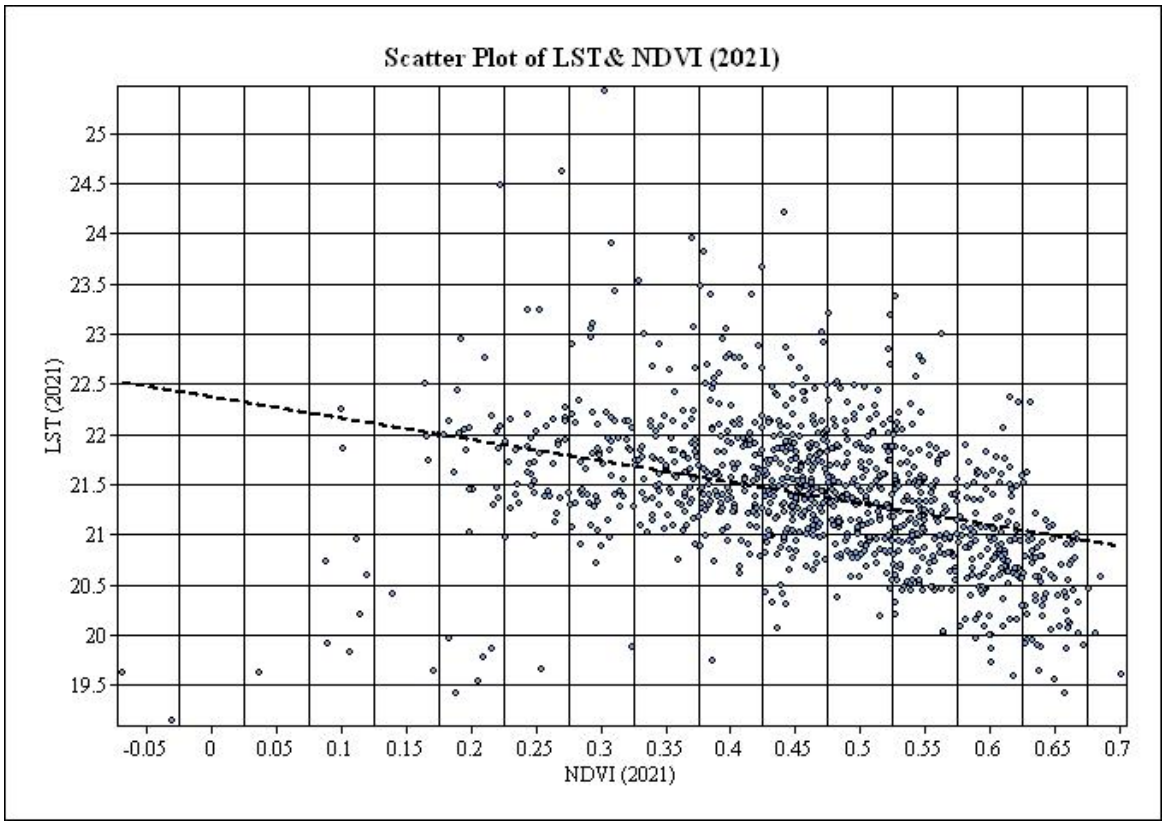

Fig. 10. Comparative analysis: NDVI and LST scatter plot (2021).

Table 9: Key Information on class level matrices.

LULC Class	PLAND (1991)	PLAND (2021)	(NP)1991	(NP)2021	(PD)1991	(PD)2021	MPS (1991)	MPS (2021)	(LPI)1991	(LPI)2021	(LSI) 1991	(LSI)2021
Agriculture	78.77	52.49	289	1261	0.93	4.05	84.89	12.96	75.57	6.89	26.89	55.72
Built-up	1.88	8.31	629	1708	2.02	5.48	0.93	1.52	0.07	0.47	28.84	49.74
Current Fallow	6.02	28.75	1139	2797	3.66	8.98	1.65	3.2	0.4	2.65	38.1	66.65
Plantation and Forest	10.58	7.21	1654	2007	5.31	6.44	1.99	1.12	0.43	0.2	49.86	52.03

Sand Bar	0.04	0.01	6	18	0.02	0.06	1.98	0.25	0.01	0	4.3	4.36
Water Bodies	2.7	3.22	170	424	0.55	1.36	4.96	2.37	0.82	0.35	18.51	27.32

Plantation and forest areas have decreased in PLAND from 10.58% to 7.21%, with NP increasing from 1,654 to 2,007 and PD from 5.31 to 6.44 indicating fragmentation. The MPS decreased from 1.99 km^2 to 1.12 km^2, and the LPI fell from 0.43% to 0.2% suggesting smaller and less dominant patches. The LSI increased slightly from 49.86 to 52.03 indicating more complex patch shapes. Sand bars have seen a reduction in PLAND from 0.04% to 0.01%, with NP increasing from 6 to 18 and PD from 0.02 to 0.06. The MPS decreased significantly from 1.98 km^2 to 0.25 km^2, and the LPI became negligible dropping from 0.01% to 0%. The LSI shows a slight increase from 4.3 to 4.36 indicating that sand bars have become more fragmented and irregular. Water bodies have experienced a slight increase in PLAND from 2.7% to 3.22%, with NP rising from 170 to 424 and PD from 0.55 to 1.36. The MPS decreased from 4.96 km^2 to 2.37 km^2, and the LPI fell from 0.82% to 0.35%. The LSI increased from 18.51 to 27.32, indicating more fragmentation and complexity in water body patches. The analysis of landscape fragmentation from 1991 to 2021, incorporating Shannon's Diversity Index (SHDI), highlights notable trends in land use and ecological diversity. SHDI increased from 0.7703 in 1991 to 1.205 in 2021, indicating a rise in landscape heterogeneity and patch diversity. This increase in SHDI suggests that the landscape has become more diverse over time, reflecting changes in land cover types and their distribution. In general, the landscape has undergone significant transformations, driven by factors such as built-up expansion, changes in agricultural practices, anthropogenic disturbances and environmental changes. These trends highlight the need for effective conservation and land management strategies to maintain ecological balance and promote sustainable land use.

Conclusion

An examination of the land cover and land use changes in Domkal Block over the past 30 years shows notable shifts brought about by a complex interaction of environmental, demographic, and socioeconomic factors. Simple change analysis is insufficient to capture the nuances of these changes; Therefore, a thorough grasp of the dynamics at work was made possible by change vector analysis and the creation of change transition matrices using ArcGIS 10.5. The study showed substantial decreases in agricultural land and plantation areas by 80.77 km^2 and 11.03 km^2, respectively, with a corresponding increase in built-up land and aquatic bodies by 19.86 km^2 and 1.6 km^2. The Domkal block, covering approximately 311 km^2, experienced nearly 44% land cover change, mostly as a result of the growth of existing fallow land, built-up areas, and plantations. Due to population pressure and a move away from traditional agricultural methods, there has been a significant encroachment of built-up areas on agricultural and plantation lands. The research highlighted a notable rise in land surface temperature (LST) over time, from 17-23°C in 1991 to 18-26°C in 2021. A statistically significant difference in LST was confirmed by the paired samples t-test, with high temperatures observed in the majority of built-up areas, bare terrain, and agricultural lands next to rivers. The presence of brick kiln factories further exacerbated these temperature increases. Fragmentation analysis, employing class level and landscape level matrices, demonstrated significant alterations in land cover categories. Agricultural land has become more fragmented and less dominant, while built-up areas have expanded and become more complex in shape. Current fallow land has increased substantially, indicating shifts in land use practices. Plantation and forest areas have decreased, becoming more fragmented and less dominant. Water bodies have also become more fragmented and complex. The landscape fragmentation analysis, incorporating Shannon's Diversity Index (SHDI) indicated a rise in landscape heterogeneity and patch diversity from 1991 to 2021. These trends reflect changes in land cover types and their distribution, driven by built-up expansion, changes in agricultural practices, anthropogenic disturbances, and environmental changes. Overall, the findings underscore the need for effective conservation and sustainable land management strategies to maintain

ecological balance and promote sustainable land use in Murshidabad district. Addressing the challenges posed by population pressure, shifting agricultural practices, and environmental changes will be crucial for achieving long-term sustainability in the region.

Acknowledgments

The first author of this study gratefully acknowledges the University Grants Commission (UGC), New Delhi, India, for providing the Senior Research Fellowship (SRF) during this research. The authors also express their gratitude to Aliah University, Kolkata for offering a conducive research environment. Additionally, the authors are thankful to the US Geological Survey (USGS) for making Landsat data freely accessible. Special thanks are extended to the editor(s) and anonymous reviewer(s) for their valuable comments and suggestions, which significantly enhanced the manuscript.

Funding

No significant financial support has been received for this work

Conflict of interest

The authors declare that they have no financial or personal interests that could influence the results or the content of this research paper.

References

Alam, N., Saha, S., Gupta, S. and Chakraborty, S., 2021. Prediction modelling of riverine landscape dynamics in the context of sustainable management of floodplain: a Geospatial approach. Annals of GIS, 27(3), 299-314. https://doi.org/10.1080/19475683.2020.1870558

Artis, D.A., and Carnahan, W.H., 1982. Survey of emissivity variability in thermography of urban areas. Remote Sensing of Environment, 12(4), 313-329. https://doi.org/10.1016/0034-4257(82)90043-8

Bety, A., 2013. Urban geomorphology of Sulaimani City, using remote sensing and GIS techniques, Kurdistan Region, Iraq. Unpublished PhD thesis, Faculty of Science and Science Education, University of Sulaimani, 125. https://doi.org/10.46717/igj.57.2C.17ms-2024-9-25

Bhatta, B., 2008. Remote sensing and GIS. Oxford University Press.

Borthwick, R., de Flamingh, A., Hesselbarth, M.H., Parandhaman, A., Wagner, H.H. and Abdel Moniem, H.E., 2020. Alternative quantifications of landscape complementation to model gene flow in banded longhorn beetles [Typocerus v. velutinus (Olivier)]. Frontiers in Genetics, 307. https://doi.org/10.3389/fgene.2020.00307

Bose, A. and Chowdhury, I.R., 2020. Monitoring and modeling of spatio-temporal urban expansion and land-use/land-cover change using markov chain model: a case study in Siliguri Metropolitan area, West Bengal, India. Modeling Earth Systems and Environment, 6, 2235-2249. https://doi.org/10.1007/s40808-020-00842-6

Butt, A., Shabbir, R., Ahmad, S.S. and Aziz, N., 2015. Land use change mapping and analysis using Remote Sensing and GIS: A case study of Simly watershed, Islamabad, Pakistan. The Egyptian Journal of Remote Sensing and Space Science, 18(2), 251-259. https://doi.org/10.1016/j.ejrs.2015.07.003

Buyadi, S.N.A., Mohd, W.M.N.W. and Misni, A., 2013. Green spaces growth impact on the urban microclimate. Procedia-Social and Behavioral Sciences, 105, 547-557. https://doi.org/10.1016/j.sbspro.2013.11.058

Cheruto, M.C., Kauti, M.K., Kisangau, D.P. and Kariuki, P.C., 2016. Assessment of land use and land cover change using GIS and remote sensing techniques: a case study of Makueni County, Kenya. https://doi.org/10.4172/2469-4134.1000175

Choudhury, D., Das, K. and Das, A., 2019. Assessment of land use land cover changes and its impact on variations of land surface temperature in Asansol-Durgapur Development Region. The Egyptian Journal of Remote Sensing and Space Science, 22(2), 203-218. https://doi.org/10.1016/j.ejrs.2018.05.004

Chowdhury, M., Hasan, M.E. and Abdullah-Al-Mamun, M., 2020. Land use/land cover change assessment of Halda watershed using remote sensing and GIS. The Egyptian Journal of Remote Sensing and Space Science, 23(1), 63-75. https://doi.org/10.1016/j.ejrs.2018.11.003

Das, S. and Angadi, D.P., 2020. Land use-land cover (LULC) transformation and its relation with land surface temperature changes: A case study of Barrackpore Subdivision, West Bengal, India. Remote Sensing Applications: Society and Environment, 19, 100322. https://doi.org/10.1016/j.rsase.2020.100322

Dasgupta, A., Kumar, U. and Ramachandra, T., 2009. Urban Landscape analysis through spatial metrics. Proceedings of International Conference on Infrastructure, Sustainable Transportation and Urban Planning, (CISTUP@ CiSTUP), Indian Institute of Science, Bangalore, India,

Dewan, A.M., Yamaguchi, Y. and Ziaur Rahman, M., 2012. Dynamics of land use/cover changes and the analysis of landscape fragmentation in Dhaka Metropolitan, Bangladesh. GeoJournal, 77, 315-330. https://doi.org/10.1007/s10708-010-9399-x

Ding, H. and Shi, W., 2013. Land-use/land-cover change and its influence on surface temperature: a case study in Beijing City. International Journal of Remote Sensing, 34(15), 5503-5517. https://doi.org/10.1080/01431161.2013.792966

Gardner, R.H., O'Neill, R.V. and Turner, M.G., 1993. Ecological implications of landscape fragmentation. Springer. https://doi.org/10.1007/978-1-4612-0905-8_17

Gharaibeh, A., Shaamala, A., Obeidat, R. and Al-Kofahi, S., 2020. Improving land-use change modeling by integrating ANN with Cellular Automata-Markov Chain model. Heliyon, 6(9). https://doi.org/10.1016/j.heliyon.2020.e05092

Herold, M., Scepan, J. and Clarke, K.C., 2002. The use of remote sensing and landscape metrics to describe structures and changes in urban land uses. Environment and planning A, 34(8), 1443-1458. https://doi.org/10.1068/a3496

Hoque, I. and Lepcha, S.K., 2020. A geospatial analysis of land use dynamics and its impact on land surface temperature in Siliguri Jalpaiguri development region, West Bengal. Applied Geomatics, 12(2), 163-178. https://doi.org/10.1007/s12518-019-00288-1

Hua, A., 2017. Application of CA-Markov model and land use/land cover changes in Malacca River watershed, Malaysia. Applied Ecology and Environmental Research, 15(4). DOI: http://dx.doi.org/10.15666/aeer/1504_605622

Islam, K., Jashimuddin, M., Nath, B. and Nath, T.K., 2018. Land use classification and change detection by using multi-temporal remotely sensed imagery: The case of Chunati wildlife sanctuary, Bangladesh. The Egyptian Journal of Remote Sensing and Space Science, 21(1), 37-47. https://doi.org/10.1016/j.ejrs.2016.12.005

Kafy, A.A., Faisal, A.-A., Sikdar, S., Hasan, M., Rahman, M., Khan, M.H. and Islam, R., 2020. Impact of LULC changes on LST in Rajshahi district of Bangladesh: a remote sensing approach. Journal of Geographical Studies, 3(1), 11-23. https://doi.org/10.21523/gcj5.19030102

Kamusoko, C. and Aniya, M., 2007. Land use/cover change and landscape fragmentation analysis in the Bindura District, Zimbabwe. Land Degradation and Development, 18(2), 221-233. https://doi.org/10.1002/ldr.761

Kangabam, R.D., Selvaraj, M. and Govindaraju, M., 2019. Assessment of land use land cover changes in Loktak Lake in Indo-Burma Biodiversity Hotspot using geospatial techniques. The Egyptian Journal of Remote Sensing and Space Science, 22(2), 137-143. https://doi.org/10.1016/j.ejrs.2018.04.005

Keitt, T.H., Urban, D.L. and Milne, B.T., 1997. Detecting critical scales in fragmented landscapes. Conservation ecology, 1(1). https://www.jstor.org/stable/26271642

Landsat Project Science Office., 2002. Landsat 7 Science Data User's Handbook. NASA. Retrieved 10 September 2003.

Liu, H. and Weng, Q., 2008. Seasonal variations in the relationship between landscape pattern and land surface temperature in Indianapolis, USA. Environmental Monitoring and Assessment, 144, 199-219. https://doi.org/10.1007/s10661-007-9979-5

McGarigal, K., Cushman, S., Neel, M. and Ene, E., 2002. FRAGSTATS: spatial pattern analysis program for categorical maps. University of Massachusetts, Amherst. In. http://www.umass.edu/landeco/research/fragstats/fragstats.html

Mishra, P.K., Rai, A. and Rai, S.C., 2020. Land use and land cover change detection using geospatial techniques in the Sikkim Himalaya, India. The Egyptian Journal of Remote Sensing and Space Science, 23(2), 133-143. https://doi.org/10.1016/j.ejrs.2019.02.001

Mustaquim, M. and Islam, W. 2023. Multitemporal Analysis of Land Use/Cover Changes and Landscape Fragmentation in Murshidabad District of West Bengal, India. Current World Environment, 18(2), 647-661. https://doi.org/https://dx.doi.org/10.12944/CWE.18.2.18

Mustaquim, M. and Islam, W., 2024. Analysing Land Use and Cover Transformations in Berhampore, West Bengal, India: A CA-Markov and ANN Simulation Approach for Future Predictions. Agric Res. https://doi.org/10.1007/s40003-024-00745-3

Naqvi, H.R., Siddiqui, L., Devi, L. M. and Siddiqui, M.A., 2014. Landscape transformation analysis employing compound interest formula in the Nun Nadi Watershed, India. The Egyptian Journal of Remote Sensing and Space Science, 17(2), 149-157. https://doi.org/10.1016/j.ejrs.2014.09.001

Nelson, S.A. and Khorram, S., 2018. Image processing and data analysis with ERDAS IMAGINE®. CRC Press.

Prathamesh Barane, G.S.D., 2017. RSandGIS Plugins. In (Version 1.2)

Rehman, A., Qin, J., Pervez, A., Khan, M. S., Ullah, S., Ahmad, K. and Rehman, N.U., 2022. Land-use/land cover changes contribute to land surface temperature: a case study of the Upper Indus Basin of Pakistan. Sustainability, 14(2), 934. https://doi.org/10.3390/su14020934

Roy, B. and Kasemi, N., 2021. Monitoring urban growth dynamics using remote sensing and GIS techniques of Raiganj Urban Agglomeration, India. The Egyptian Journal of Remote Sensing and Space Science, 24(2), 221-230. https://doi.org/10.1016/j.ejrs.2021.02.001

Rwanga, S.S. and Ndambuki, J.M., 2017. Accuracy assessment of land use/land cover classification using remote sensing and GIS. International Journal of Geosciences, 8(04), 611. DOI: 10.4236/ijg.2017.84033

Saber, A., El-Sayed, I., Rabah, M. and Selim, M., 2021. Evaluating change detection techniques using remote sensing data: Case study New Administrative Capital Egypt. The Egyptian Journal of Remote Sensing and Space Science, 24(3), 635-648. https://doi.org/10.1016/j.ejrs.2021.03.001

Sánchez Sánchez, Y., Martínez Graña, A., Santos-Francés, F., Reyes Ramos, J.L. and Criado, M., 2021. Multitemporal analysis of land use changes and their effect on the landscape of the jerte valley (Spain) by remote sensing. Agronomy, 11(8), 1470. https://doi.org/10.3390/agronomy11081470

Sertel, E., Topaloğlu, R.H., Şallı, B., Yay Algan, I. and Aksu, G.A., 2018. Comparison of landscape metrics for three different level land cover/land use maps. ISPRS International Journal of Geo-Information, 7(10), 408. https://doi.org/10.3390/ijgi7100408

Seto, K.C. and Fragkias, M., 2005. Quantifying spatiotemporal patterns of urban land-use change in four cities of China with time series landscape metrics. Landscape Ecology, 20, 871-888. https://doi.org/10.1007/s10980-005-5238-8

Singh, S.K., Pandey, A.C. and Singh, D., 2014. Land use fragmentation analysis using remote sensing and Fragstats. Remote sensing applications in environmental research, 151-176. https://doi.org/10.1007/978-3-319-05906-8_9

Sisodia, P.S., Tiwari, V. and Kumar, A., 2014. Analysis of supervised maximum likelihood classification for remote sensing image. International conference on recent advances and innovations in engineering (ICRAIE-2014), https://doi.org/10.1109/ICRAIE.2014.6909319

Snyder, W.C., Wan, Z., Zhang, Y. and Feng, Y.Z., 1998. Classification-based emissivity for land surface temperature measurement from space. International Journal of Remote Sensing, 19(14), 2753–2774. https://doi.org/10.1080/014311698214497

Townshend, J.R. and Justice, C., 1986. Analysis of the dynamics of African vegetation using the normalized difference vegetation index. International Journal of Remote Sensing, 7(11), 1435-1445. https://doi.org/10.1080/01431168608948946

Wu, J., 2008. Land use changes: Economic, social, and environmental impacts. Choices, 23(4), 6-10.

Zhang, Y., Balzter, H., Liu, B. and Chen, Y., 2016. Analyzing the impacts of urbanization and seasonal variation on land surface temperature based on subpixel fractional covers using Landsat images. IEEE Journal of Selected Topics in Applied Earth Observations and Remote Sensing, 10(4), 1344-1356. https://doi.org/10.1109/JSTARS.2016.2608390

Ziaul, S. and Pal, S., 2016. Image based surface temperature extraction and trend detection in an urban area of West Bengal, India. Journal of Environmental Geography, 9(3-4), 13-25. https://doi.org/10.1515/jengeo-2016-0008